Thesis Proposal, October 2013

Search for New Physics in the Exclusive Delayed $\gamma + \not\!\!E_T$ Final State from $p\bar{p}$ Collisions with $\sqrt{s} = 1.96$ TeV at CDF

Vaikunth Thukral
Texas A&M University, USA
(Dated: October 17, 2013)

Theories predicting new physics beyond the Standard Model give a compelling reason to study high energy $p\bar{p}$ collisions for particular final states using experiments like the Collider Detector at Fermilab (CDF). Amongst these theories is Supersymmetry (SUSY), and we can search for evidence for SUSY particles in nature by considering events in the Delayed Photon + Missing Transverse Energy final state. Recent studies suggest a potential excess of such events beyond Standard Model predictions. With an improved set of calibrations and background estimation methods, we are in a position to utilize the remaining 30% of the data collected by CDF, and answer any remaining questions brought up by previous results as well as estimate our sensitivity to SUSY models.

INTRODUCTION

The unknown [1] nature of possible new particles or interactions motivates search strategies at particle collider experiments like the Tevatron by seeking deviations from standard-model (SM) expectations [2]. One way to search for such deviations is by looking for massive, neutral, long-lived particles decaying to energetic photons that can be seen in detectors like the CDF [3]. For example, in gauge-mediated supersymmetry-breaking (GMSB) scenarios [4], the lightest neutralino (supersymmetric partner of the standard-model gauge bosons) can be produced during proton-antiproton ($p\bar{p}$) collisions in the center of the detector, and then decay-in-flight into a photon and a stable gravitino (supersymmetric partner of the hypothesized graviton). If the neutralino has a sizeable mass and lifetime, the photon from the neutralino decay can traverse inside the detector and have an arrival time at the calorimeter later than would be expected for a photon from prompt production (*delayed* photon) [5], as seen in Fig 1. If the gravitino is non-interacting, it escapes the detector without depositing energy, providing a smoking-gun missing energy signature. By looking for and counting such collisions, a comparison with the expected number of events from known sources at a given time can be made.

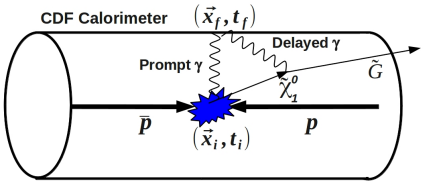

FIG. 1. A schematic of production of long-lived $\tilde{\chi}_1^0$ at the Tevatron decaying to a Gravitino ($\tilde{G}$) and a photon (γ) inside the CDF detector with the photon arriving with a delayed time.

Many previous searches have focused on SPS-8 GMSB models [6], where the neutralino is produced in cascade decays, but have all returned null results [7, 8]. Direct pair-production of neutralinos can proceed via different mechanisms, including processes that involve single Higgs-boson production, and can evade current bounds [9]. The search sensitivity in such scenarios, with nanosecond $\tilde{\chi}_1^0$ lifetimes, can be improved by studying final states in which only one of the neutralinos decays within the detector, resulting in an exclusive final state with a delayed photon and missing transverse energy [5, 9, 10].

This draft follows up on the first such search that was done for the exclusive production of events with a delayed photon and $\not\!\!E_T$ signature [11] using 6.3 fb^{-1} at CDF, as well as summarizes future plans for improving the sensitivity of the overall result. The full data analysis will be able to use up to 9.6 fb^{-1} of integrated luminosity from $p\bar{p}$ collisions collected with the CDF detector through Run II at the Fermilab Tevatron [11].

In the forthcoming sections, a summary of theoretical motivations for this study will be presented. Information about the CDF detector itself that is relevant to the measurements needed for the analysis will be discussed, followed by a brief history of the old results. We conclude with a description of the proposed improvements in calibrations as well as the background estimation for the full analysis and limit setting plans.

MOTIVATION

The Standard Model (SM) has been the most successful and prominent theory for describing observations in data from collider experiments. With the recent discovery of the final piece of the SM puzzle at the LHC [12], the Higgs boson, the search for physics beyond the Standard Model has become more focused. This is because

the SM, albeit successful, still has many incongruities with some observations, which means that it is not necessarily a complete explanation of experiments and that there may be more particles or new interactions yet to discover.

In particular, the Standard Model suffers from a "hierarchy" problem where calculation of the Higgs mass diverges. The contributions to the mass calculation can come from the Higgs' couplings to fermions, and since it couples strongest with heavier particles, the biggest contribution would come from the top quark. These corrections look like:

$$\Delta m_H^2 = -\frac{|\lambda_f|^2}{8\pi^2}[\Lambda_{\rm UV}^2 + ...] \quad (1)$$

where $\Lambda_{\rm UV}^2$ is the ultraviolet cut-off scale, and λ_f is the coupling strength of the Higgs to said fermion. If we take the ultraviolet cutoff scale to be the Planck scale, these corrections diverge very quickly. This is contrary to observations made recently [12] of a boson of mass 125 GeV and properties of the Standard Model Higgs [13].

In order to circumvent this, one possible solution is to introduce additional terms to keep the mass at finite values [14]. The introduction of these terms is what gives motivation for Minimal Supersymmetric Standard Model (MSSM), wherein each fermion has a bosonic superpartner, and each boson has a fermionic superpartner. These superpartners contribute with opposing signs to the mass corrections, suppressing the divergence.

However, no SUSY particles have been observed despite multiple analyses searching for varied scenarios [15]. In this analysis, we focus on the Light Neutralino and Gravitino (LNG) scenario of Gauge Mediated Supersymmetry Breaking (GMSB), which is not yet ruled out and has the potential for yielding interesting results at CDF. In this scenario, the NLSP (Next to Lightest SUSY Particle) which is the Neutralino is restricted to be lighter than a Z boson, that can decay to the Gravitino, which is the LSP (Lightest SUSY particle). The lifetime of this decay depends on certain parameters [9], and in certain models a lifetime that is of the order of nanoseconds is favored because of the small couplings between the two particles.

Since new particle production, as shown in Fig 2, can produce pairs of neutralinos that can decay to photons and the gravitino, this can lead to signatures that can be studied at collider experiments. The gravitino, being weakly interacting will leave the detector, appearing as a $\not\!\!E_T$ signature, and the photon will be recorded as an energy deposit in the calorimeter. In the case of a long lifetime of the neutralinos, many can leave the detector without interacting. For those that travel significantly, but not outside the detector, the photon also has a delayed time signature due to the long lifetime of the neutralino, hence leaving the $\gamma_{delayed} + \not\!\!E_T$ signature.

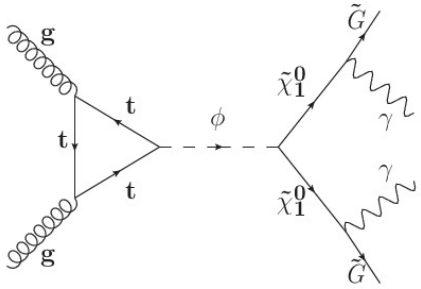

FIG. 2. A Feynman diagram illustrating neutral scalar production decaying into a SUSY $\tilde{\chi}_1^0$ $\tilde{\chi}_1^0$ pair which, in the simplest GMSB models, can produce a signal of a delayed photon and Missing Transverse Energy ($\not\!\!E_T$).

A recent search using 6.3 fb^{-1} of data from CDF Run II [16] in this final state had a result that was 1.2σ deviations from Standard Model predictions. This provides additional motivation for a follow-up study using more data and better techniques, and will be the topic of this thesis.

EXPERIMENTAL TOOLS

Detailed descriptions of the CDF II detector can be found in the references [17]. The detector subsystems relevant to this analysis are briefly mentioned here. The event kinematic properties and detector geometry are described in a cylindrical coordinate system [10]. The detector is composed of a silicon microstrip tracking system ("silicon vertex detector"), a tracking drift chamber, a calorimeter detector, and a muon detector. The silicon vertex detector provides a high-precision position measurement of charged particle trajectories, while the drift chamber provides accurate momentum measurements and allows the reconstruction of each charged particle's production time.

The combination of these measurements provides accurate reconstruction of the position ($\vec{x}_{\rm i}$) and time ($t_{\rm i}$) of the primary $p\bar{p}$ interaction vertex. The $p\bar{p}$ luminous region is approximately described by Gaussian distributions centered at $z_{\rm i} = 0$ with an rms spread of 28 cm and mean time of $t_{\rm i} = 0$ with an rms spread of 1.28 ns. The calorimeter has a pointing-tower geometry and is composed of separate electromagnetic and hadronic compartments that are used to identify photons, electrons, jets, and muons, and measure the $\not\!\!E_T$ in the event. The measurement of the arrival time ($t_{\rm f}$) of photons (and electrons) in the electromagnetic calorimeter is done using the EMTiming system and has a resolution of 0.60 ns [18].

The CDF experiment uses a multi-trigger online data acquisition system. This analysis uses events selected with a trigger that requires events with a photon candidate having at least 25 GeV of E_T, as well as a re-

quirement of at least 25 GeV of $\not\!\!E_T$ in the event. By allowing several additional photon triggers, we achieve approximately 100% efficiency for events passing the final selection requirements [7].

In the offline analysis, photon candidates are required to meet standard photon identification requirements with a minor modification as described in Ref. [7]. The offline photon E_T and event $\not\!\!E_T$ values are calculated with respect to the center of the detector ($\not\!\!E_T^0$) rather than the selected primary vertex. To suppress background sources (described below and listed in Table I), both the photon E_T and event $\not\!\!E_T$ are required to be greater than 45 GeV. Backgrounds from non-collision sources, from cosmic rays and beam-halo sources, are rejected using standard criteria [7, 19], supplemented by new requirements. Collectively, these criteria reduce the beam-halo backgrounds to a negligible level, and the data is dominated by collision and cosmic-ray background sources.

The $p\bar{p}$ interaction position and time are reconstructed using an algorithm that combines well measured tracks to form a candidate vertex [7]. Vertex candidates must have at least three high-quality tracks that intersect each other within 1.5 cm along the z-axis and within 1.5 ns in time, with $\Sigma p_T \geq 5$ GeV and $|z| < 60$ cm, where Σp_T is the scalar sum of the transverse momenta of the corresponding charged particles. If multiple vertices are reconstructed in the event, the vertex with the highest Σp_T is selected as the primary vertex. The reconstructed vertices use the average z and t of the tracks, and have a spatial and temporal resolution of 0.24 cm and 0.22 ns respectively.

OVERVIEW OF THE ANALYSIS

As mentioned earlier, the backgrounds for this analysis can be categorized as collision and non-collision backgrounds, i.e., background events whose source is at the $p\bar{p}$ interaction and unrelated to the collision respectively. A full list of backgrounds is listed in Table I. Collision backgrounds to the exclusive $\gamma + \not\!\!E_T$ final state result from processes of γ + jets production, where an unreconstructed jet mimics $\not\!\!E_T$; $Z\gamma \to \nu\nu\gamma$ production; $W \to l\nu$ production, where the lepton or an extraneous jet is misidentified as a photon; and $W(\gamma) \to l\nu\gamma$ production, where the lepton is not identified. The non-collision backgrounds are primarily cosmic-ray events [7], which are high energy muons that constantly bombard the detector leaving energy deposits. Requiring the exclusive $\gamma+\not\!\!E_T$ final state rejects most of these backgrounds. Any event with a reconstructed track with $p_T > 10$ GeV/c and pseudorapidity $|\eta| < 1.6$ [10] is excluded from the analysis since it likely came from an electron or muon. Similarly, events are rejected if they contain an additional energy cluster, reconstructed with the JETCLU [20] algorithm with a $\Delta R = 0.4$ cone, with $E_T > 15$ GeV, leaving us with a sample consisting of mostly photon candidates.

Standard Model Collision Sources
$W \to e\nu \to \gamma_{\rm fake} + \not\!\!E_T$
$\gamma + {\rm jet} \to \gamma + {\rm jet}_{\rm lost} \to \gamma + \not\!\!E_{T\,\rm fake}$
$W\gamma \to l\nu\gamma \to \gamma + l_{\rm lost} + \not\!\!E_T$
$W \to \mu\nu \to \gamma_{\rm fake} + \not\!\!E_T$
$W \to \tau\nu \to \gamma_{\rm fake} + \not\!\!E_T$
$Z\gamma \to \nu\nu\gamma \to \gamma + \not\!\!E_T$
Non-Collision Sources
Cosmics
Beam Halo
Satellite Bunches

TABLE I. Standard model and non-collision backgrounds for the exclusive $\gamma + \not\!\!E_T$ search.

An important variable in this search is the difference between the observed arrival time of a photon in the detector and the time predicted for photons promptly produced in the primary $p\bar{p}$ interaction. This difference in time, $t_{\rm corr}$, is used to distinguish signal candidate events from background sources. For each such photon candidate we calculate:

$$t_{\rm corr} = (t_{\rm f} - t_{\rm i}) - \frac{(|\vec{x}_{\rm f} - \vec{x}_{\rm i}|)}{c} \qquad (2)$$

where $(|\vec{x}_{\rm f} - \vec{x}_{\rm i}|)/c$ is the expected time-of-flight (TOF) of a prompt photon from the selected $p\bar{p}$ interaction vertex to the location of the associated energy deposit in the calorimeter. For a promptly-produced photon, and with perfect measurements, $t_{\rm corr} = 0$ ns. The signal region for this analysis is where we expect delayed photons to appear from possible new physics processes with sufficient reduction in background, and is defined as $2 < t_{\rm corr} < 7$ ns. By picking this time, most promptly produced photons at small values of $t_{\rm corr}$ are removed. In addition, contributions from background sources at larger times (like cosmic-ray events) are also reduced. Using this variable, a simple counting of the number of collisions in data that produce delayed photons can be made in the aforementioned signal region to be compared with expected production of such photons from known background sources.

Since the calculation of $t_{\rm corr}$ depends heavily on measuring the time and position of the initial point of interaction, the collision backgrounds can further be divided into two classes of events. The first class includes events in which the photon is correctly associated with its production vertex; these events are reduced by the final timing requirement and are called "*Right-Vertex*" events. The second class includes events in which the primary vertex is incorrectly selected as the production vertex of the photon, called "*Wrong-Vertex*" events. Each

collision background event is classified as a right vertex or a wrong vertex event regardless of the number of extra collisions in the event. The goal of the background estimation is to account for all these main sources together. The dominant collision background in the signal region, $(2, 7)$ ns, comes from prompt SM-photon production events with a wrong vertex, and after selection requirements, backgrounds from non-collision sources are dominated by cosmic-ray sources.

The $t_{\rm corr}$ distributions for right vertex and wrong vertex events are both well modeled by Gaussian distributions after all selection requirements [18]. The distribution describing right vertex events is well described by an RMS of 0.65 ns and a mean centered (with some uncertainty) around 0 ns, reflecting contributions of the vertex-reconstruction algorithm and the calorimeter-timing resolutions [18]. The distribution describing wrong vertex collision events has an RMS spread of 2.0 ns [18]. Its mean depends on the associated SM processes and cannot be assumed *a priori*. Since the collision-background timing distribution is described by the sum of the right vertex and wrong vertex event distributions, the collective collision background is modeled by the sum of two Gaussian distributions. The normalizations for the right vertex and wrong vertex event distributions, as well as mean $t_{\rm corr}$ for each distribution, are determined using data and a sophisticated procedure described below.

Finally, since the cosmic-rays arrive flat in time and are uniform, their rate is estimated away from the collision time, from $20 < t_{\rm corr} < 80$ ns, by averaging over the number of events observed per ns. With these background sources combined, a potential signal would then appear as an excess over the total number of expected events in the signal region, simulated as in Fig 3.

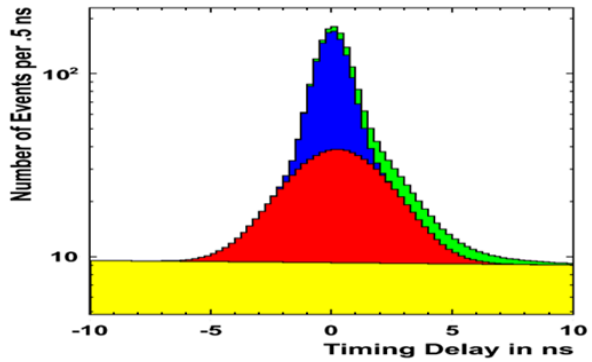

FIG. 3. A toy simulation of t_{corr} including GMSB signal events (green) along with a set of collision events. Here the right vertex (blue), wrong vertex (red), and cosmic ray (yellow) distributions are shown for completeness.

Three main effects introduce process-specific non-Gaussian tails and $\mathcal{O}(100$ ps) biases on the mean of the wrong vertex timing distribution. We make additional event requirements that remove most pathological cases of the mean shifts and measure the remaining amount of bias.

The first is a threshold effect that affects events with the photon E_T near the analysis's threshold of 45 GeV. Use of the wrong vertex position in photon kinematic reconstruction biases the measured value of the photon transverse energy ($E_T^{\rm m}$) with respect to its true value ($E_T^{\rm t}$) for geometric reasons. If the selection of the wrong vertex results in a shorter path length from the collision to the calorimeter, then E_T is overestimated. Similarly, an event with longer path length will have E_T that is underestimated. Thus, an E_T threshold biases the $t_{\rm corr}$ distribution towards positive $t_{\rm corr}$ values. This threshold bias effect is minimized by computing E_T (and $\not\!\!E_T$ for consistency) from the center of the detector ($z = 0$).

Second, we only select events where the primary vertex is observed to have $|z| < 60$ cm. Events with photons from collisions originating with $|z| > 60$ cm would necessarily have the wrong vertex used to compute E_T and $t_{\rm corr}$. This induces a positive bias in the timing. For this reason, all events with a vertex (but using a less restrictive vertex identification algorithm) with $|z| > 60$ cm are rejected [21]. This requirement is 95% efficient for events with a correctly-reconstructed primary vertex satisfying $|z| < 60$ cm.

The last significant effect is from $W \to e\nu$ events identified as $\gamma + \not\!\!E_T$ in a way that biases $\langle t_{\rm corr}\rangle$ towards positive values. In this case, as the electron traverses the tracking system, it loses most of its energy to a high-energy photon via bremsstrahlung. As the trajectory of the low-energy electron is curved away from the final photon direction, the photon candidate passes all the photon-identification criteria. By requiring that there be no tracks around the energy deposit in a cone of $\Delta R < 5.0$ (in $\eta - \phi$ space), events in which the electron track does not point to the photon position in the calorimeter can be rejected. Studies show that this requirement is approximately 95% efficient for prompt photons and reduces the background rate from this source by about 70%.

The Gaussian distribution that describes the timing distribution for wrong vertex events is summed with the Gaussian distribution for right vertex events to fully model the collision background. The six parameters for the mean, rms spread, and normalization of these two distributions uniquely determine the expected event yield from collision backgrounds in the signal region. Most of the parameters, including the rate of cosmic-ray events, are directly determined from the $\gamma+\not\!\!E_T$ candidate event data sample in the region $-7 < t_{\rm corr} < 2$ ns and $20 < t_{\rm corr} < 80$ ns for events with a vertex. Both normalizations are obtained from fitting the two-Gaussian model to the data in the range $-7 < t_{\rm corr} < 2$ ns since both rms spreads are known. The one remaining parameter that must be determined separately is $\langle t_{\rm corr}^{\rm WV}\rangle$, the

mean of $t_{\rm corr}$ for wrong vertex events, which is still needed to correctly model the collision backgrounds. Fitting for the sum of the two Gaussian distributions for this parameter is not sensitive enough since the region between $-2 < t_{\rm corr} < 2$ ns is dominated by right vertex events.

To determine $\langle t^{\rm WV}_{\rm corr}\rangle$, a sample of events independent of the exclusive $\gamma + \not\!\!E_T$ sample is created. This sample of events is identical to the $\gamma + \not\!\!E_T$ sample except for a requirement that there be no reconstructed vertex. We call this a sample of *No-Vertex* events. The value of $t_{\rm corr}$ for an event that does not have a reconstructed vertex, denoted $t^0_{\rm corr}$, is computed assuming an initial time and position of $t_{\rm i} = 0$ and $z_{\rm i} = 0$ in Eqn 2. For geometric reasons, $\langle t^0_{\rm corr}\rangle = \langle t^{\rm WV}_{\rm corr}\rangle$ to a high degree of precision for the entire sample [11]. With appropriate uncertainties determined from the fit, the $t^0_{\rm corr}$ distribution is well described by a single Gaussian with an RMS spread $= 1.6 \pm 0.08$ ns and a normalization that is determined from data. This is then used as the mean of the wrong vertex distribution in a binned log likelihood fit to extrapolate into the signal region.

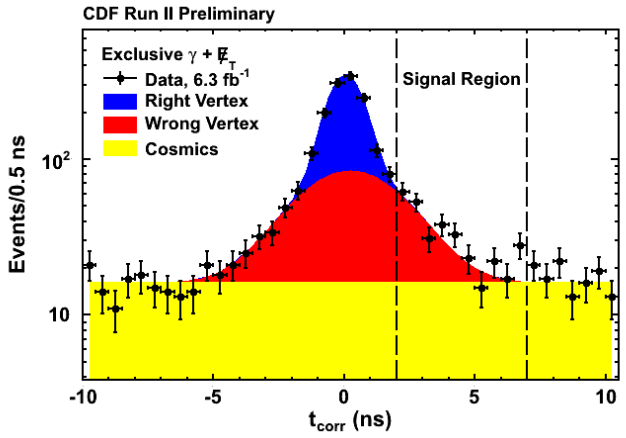

FIG. 4. The $t_{\rm corr}$ distribution, from $-10 < t_{\rm corr} < 10$ ns, and the signal region indicated by dashed lines

Using the 6.3 fb^{-1} dataset, the background estimate predicts 286 ± 24 events in the signal region, where the uncertainty is dominated by the number of events in the no vertex sample. In data there are an observed 322 events in the signal region. This corresponds to a 1.2σ significance (see Fig 4), and this result was published in PRD-RC [16].

FUTURE ANALYSIS STRATEGY

With previous results now published [16], there is now room and motivation to establish a final answer for the full CDF data taking period and to extend the results to tell us more about nature. This thesis is thus the follow up of the tools previously developed for the analysis. To do this, there are a few areas in which improvements can be made, namely:

- Improving timing calibrations
- Better background estimation
- Adding more data
- Setting limits on new physics processes ($H \rightarrow \tilde{\chi}^0_1\,\tilde{\chi}^0_1$) and potentially optimize based on lowering energy thresholds

The aforementioned steps are the main tasks that will be performed for this thesis, and the plans for performing them are are discussed in detail below.

Improving Timing Calibrations

Before we can look at the final data sample of $\gamma + \not\!\!E_T$ events, we must calibrate all the timing measurements that go into the calculation of $t_{\rm corr}$. For this, we use a large data sample with loose track requirements and validate with $W \rightarrow e\nu$ events since the final state differs from the exclusive $\gamma + \not\!\!E_T$ final state only in the charged-particle track associated with the electron. In such events, the electron track is removed from the event reconstruction to emulate exclusive $\gamma + \not\!\!E_T$ events, then used *a posteriori* to determine whether the emulated photon is correctly associated with its production vertex.. The need to calibrate tracks arises from the $t_{\rm corr}$ equation mentioned earlier (Eqn 2). The two terms, t_f and t_i, are determined from the EMTiming system and from the reconstructed vertices respectively. For t_i, since reconstructed vertices are made using an algorithm that requires the timing and position measurements of the tracks, calibrating tracks to remove correlations between track parameters leads to well measured vertices, and hence, more accurate $t_{\rm corr}$ measurements.

In the previous method used for calibrations, tracks were well-centred around zero, Gaussian-like and showed little run-by-run variations. However, the parameters over which the track times were calibrated still showed some variations in the mean track time. This means that the previous procedure calibrated the average track times to zero, but the calibration parameters still have some correlations left within them. In order to improve our sensitivity, better calibrations are required. This is done by adding a few more steps to the calibration procedure with the main goal of having mean track times centred around zero (*on average*) around $Z = 0$, and by only picking "good" tracks to calibrate over.

First, a coarse calibration, similar to the previous analysis, is done to center the mean track times around zero. The objective is to define $t_{\rm i} = 0$ to be the collision time, *on average*, for when the $p\bar{p}$ bunches collide at the center of the detector at $z_{\rm i} = 0$. This is used as a $0th$ order

correction. Next, vertices are reconstructed using these coarse tracks. They are then calibrated again relative to their best guess collision times on an event-by-event basis, i.e., only tracks that are used for reconstructing vertices are picked to center them around their respective collision time (instead of zero). By design, the vertexing algorithm discards tracks that tend to pathologically vary for large values of the calibration parameters while constructing vertices. By considering tracks matched within 3σ of the vertex for this step of the process, it allows for more accurate calibration constants.

In addition, since these tracks are already known to be associated with a vertex, the calibration constants generated for them ensure that they will be adjusted closer to their true values, and hence produce future track measurements that are also close to their true value. By doing this, a step used in the previous calibrations is also negated as there is no need to separately add further corrections to the vertices themselves, since the tracks are now "zeroed" with respect to their associated vertices. We call this a ΔT correction, and use it as the next order correction term. A comparison of the correlation of the mean track time between two calibration parameters (the impact parameter and charge over transverse momentum, which are track reconstruction variables) is shown in Fig 5.

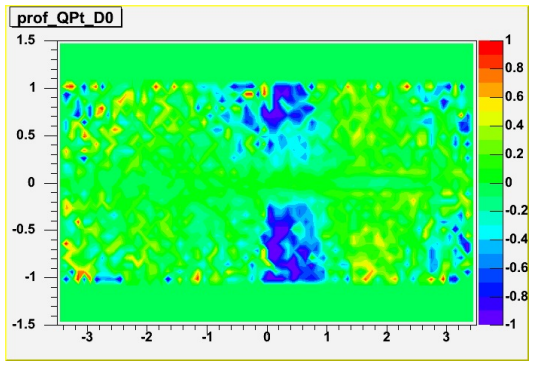

(a)

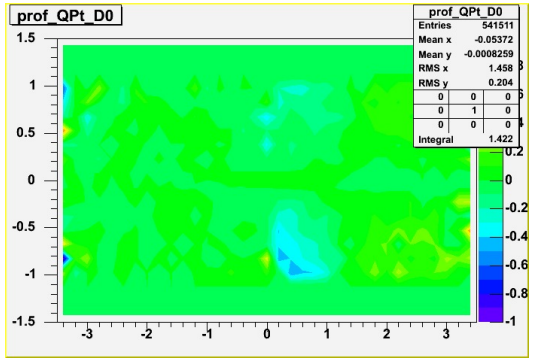

(b)

FIG. 5. Plots showing variation in mean track time for $D0$ vs Q/P_T a) before and b) after new calibrations

Lastly, one more correction is added to the track times due to $p\bar{p}$ bunches having different bunch widths during the collision [22]. These bunches are approximately described by Gaussians, and since the longitudinal profiles of the two as they pass each other are different, it leads to a correlation between the mean collision time and the Z position of the collision. This slope in the measurement of the track times, i.e., tracks at large positive values of Z tend to be at large negative times, and tracks at large negative Z tend to have large positive times, needs to be taken into account when performing our calibration procedure. Preliminary results show that this can be represented with a line (and hence an equation) that has a clear slope as well as an offset at $Z = 0$ (Fig 6). Since vertices are constructed directly from these tracks, the slope is also seen in vertex times against their Z positions. To take this into account, the mean time is set to zero for for all tracks at a Z position of zero, in line with the same objective for making the previous corrections. This correction is generated run-by-run for the entire data since the equipment timing offset is different for different runs.

To complete the overall timing calibration, updated EMTiming corrections will be generated with the better vertex timing calibrations.

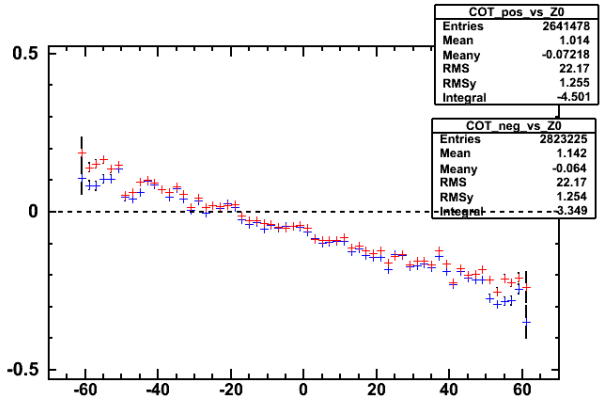

FIG. 6. The slope and offset in positive (blue) and negative (red) tracks as seen in the mean track time against Z *before* corrections

Better Background Estimation

After these calibrations are validated, the next improvement comes from a better understanding of the background estimation used in the previous analysis. As mentioned earlier, the dominant background in the data sample comes from non-collision cosmic-ray sources. These are estimated by using the data that is far away from the collision time, and extrapolated back in to the

signal region by calculating a cosmic-ray rate. This was based on the assumption that the timing distribution for cosmic rays is flat, since they actually hit the detector at a constant rate over time.

However, while the incident rate of cosmic ray events at the detector is indeed uniform in time, with higher statistics we have determined that the observed number of reconstructed cosmic ray events in the detector and passing all event requirements is not uniform as a function of time. This is due to a bias induced by not all cosmics passing selection requirements, and are hence lost in the process. This occurs because it was assumed that these losses only occurred on the edges of the energy integration window, but with more data it is observed that they instead have a slope across the collision timing regions, as seen in Fig 7. Hence, instead of using the previous estimate of averaging cosmic-ray events, the number of cosmic ray backgrounds is better described by a linear distribution with a slope that can be determined in the $20 < t_{\rm corr} < 80$ ns region.

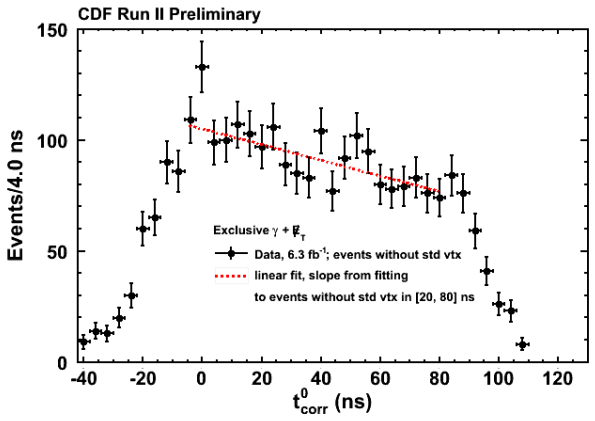

FIG. 7. Cosmic-ray events in the data sample, new rate is estimated by a slope fit instead of assuming flat production

This data shows a negative slope, as estimated using a pure sample of cosmics selected with the no-vertex sample and requiring $\Sigma Pt = 0$, the result of which means that the previous methods underestimated the number of cosmic-ray events in the signal region. Incorporating this into the full fitting procedure predicts 187 ± 8 cosmic events, instead of 159 ± 4 in the previous result; note that the extra uncertainty reflects the removal of the flat assumption. Hence, the new expected total number of events in the signal region changes to 310 ± 24, which compared to the observed 322 gives a preliminary result of 0.4σ. This shows that nearly all the excess is accounted for and there is Standard Model agreement.

Adding More Data

With these new calibration and background methodologies in place, the next step is to extend the analysis using the rest of the CDF dataset. The last result used 6.3 fb^{-1} of data. The Tevatron has delivered 10 fb^{-1}, and potentially up to 9.6 fb^{-1} can be used for the full data analysis. Adding the last bit of data should help with some of the dominant uncertainties that come from the parameters used in the background estimation fitting method (like approximating the wrong-vertex mean from the low statistics no-vertex sample).

Setting Limits on New Physics Processes

In addition, the final answer can be used to set limits on new physics production cross-section. Recent studies [23] indicate that considering the $H \rightarrow \tilde{\chi}^0_1\,\tilde{\chi}^0_1$ production and decay mode, the acceptance and the shape of the $t_{\rm corr}$ distribution depends on parameters of this signal model. The $t_{\rm corr}$ distribution in the signal region can also be described by an exponential function. With a full fit to the data, event counts and shapes of the predicted background and observation, together with the luminosity and predicted acceptance, limits on the cross-section of $p\bar{p} \rightarrow H \rightarrow \tilde{\chi}^0_1\,\tilde{\chi}^0_1$ can be calculated.

CONCLUSION

In conclusion, previous results of the first signature-based search for the production of events with the exclusive delayed $\gamma + \not\!\!E_T$ final state are used as motivation for finishing the search in replete detail. A number of novel techniques used for this search suggest that there is no evidence for new physics, but the appearance of a mild excess deserves to be followed up with more data. This can be achieved by further improvements in the methodology used in the calibrations, as well as a new estimation for the backgrounds, both of which have been discussed in the previous section. Performing these steps can improve the sensitivity of the final answer, and is motivation towards setting limits on new physics processes for a complete analysis with all these factors considered.

[1] J. D. Mason, D. E. Morrissey, and D. Poland, Phys. Rev. D **80**, 115015 (Dec 2009).
[2] S. L. Glashow, Nucl. Phys. **22**, 579 (1961); S. Weinberg, Phys. Rev. Lett. **19**, 1264 (1967); A. Salam, *Proc. 8th Nobel Symposium, Stockholm* (1979).
[3] D. Acosta *et al.* (CDF Collaboration), Phys. Rev. D **71**, 031104 (2005).

[4] M. Dine and W. Fischler, Phys. Lett. B **110**, 227 (1982); C. R. Nappi and B. A. Ovrut, *ibid.* **113**, 175 (1982); L. Alvarez-Gaumé, M. Claudson, and M. B. Wise, Nucl. Phys. **B207**, 96 (1982); S. Dimopoulos and S. Raby, *ibid.* **B219**, 479 (1983).

[5] D. A. Toback and P. Wagner, Phys. Rev. D **70**, 114032 (2004).

[6] B. Allanach *et al.*, Eur. Phys. J. C **25**, 113 (2002).

[7] A. Abulencia *et al.* (CDF Collaboration), Phys. Rev. Lett. **99**, 121801 (2007); T. Aaltonen *et al.* (CDF Collaboration), Phys. Rev. D **78**, 032015 (2008).

[8] A. Heister *et al.* (ALEPH Collaboration), Eur. Phys. J. C **25**, 339 (2002); M. Gataullin, S. Rosier, L. Xia, and H. Yang, AIP Conference Proceedings **903**, 217 (2007); G. Pásztor, PoS HEP2005 346 (2005); J. Abdallah *et al.* (DELPHI Collaboration), Eur. Phys. J. C **60**, 17 (2009); T. Aaltonen *et al.* (CDF Collaboration), Phys. Rev. Lett. **104**, 011801 (2010); V. M. Abazov *et al.* (D0 Collaboration), *ibid.* **105**, 221802 (2010); S. Chatrchyan *et al.* (CMS Collaboration), *ibid.* **106**, 211802 (May 2011); G. Aad *et al.* (ATLAS Collaboration), *ibid.* **106**, 121803 (Mar 2011); S. Chatrchyan *et al.* (CMS Collaboration), Phys.Lett. **B722**, 273 (2013).

[9] J. D. Mason and D. Toback, Phys. Lett. B **702**, 377 (2011).

[10] In the CDF II detector, a particle's direction is characterized by the azimuthal angle ϕ, the pseudorapidity $\eta = -\ln[\tan(\theta/2)]$, where the polar angle θ is measured with respect to the proton beam direction. The transverse energy E_T is defined as $E\sin\theta$, where E is the energy in the electromagnetic and hadronic calorimeter towers associated with a cluster of energy deposition. The missing transverse energy $\vec{\not\!\!E}_T$ is defined as $\vec{\not\!\!E}_T = -\Sigma_i E_T^i \vec{n}_i$, where $\vec{n}_i$ is a unit vector in the transverse plane that points from the interaction vertex to the i^{th} calorimeter tower. $\not\!\!E_T$ is the magnitude of $\vec{\not\!\!E}_T$. The cylindrical axis of the detector is denoted as the z coordinate and increases positively in the direction of the proton beam.

[11] J. Asaadi, Ph.D. thesis, Texas A&M University [2012-43]; A. Aurisano, Ph.D. thesis, Texas A&M University [2012-35].

[12] S. Chatrchyan *et al.* (CMS Collaboration), Phys. Lett. B **716**, 30 (2012); G. Aad *et al.* (ATLAS Collaboration), *ibid.* **716**, 1 (2012); T. Aaltonen *et al.* (CDF and D0 Collaborations), Phys. Rev. Lett. **109**, 071804 (2012).

[13] M. Chen (CMS Collaboration)(2013), arXiv:1305.4775; S. M. Consonni (on behalf of the ATLAS Collaboration)(2013), arXiv:1305.3315.

[14] S. Dawson (1997) arXiv:hep-ph/9712464.

[15] J. Beringer *et al.*, Phys. Rev. D **86**, 010001 (2012).

[16] T. Aaltonen *et al.* (CDF Collaboration), Phys.Rev. **D 88**, 031103 (2013).

[17] A. Abulencia *et al.* (CDF Collaboration), J. Phys. G **34**, 2457 (2007).

[18] M. Goncharov *et al.*, Nucl. Instrum. Methods **565**, 543 (2006).

[19] T. Aaltonen *et al.* (CDF Collaboration), Phys. Rev. Lett. **101**, 181602 (2008).

[20] F. Abe *et al.* (CDF Collaboration), Phys. Rev. D **45**, 1448 (1992).

[21] W. Ashmanskas *et al.*, Nucl. Instrum. Methods **477**, 451 (2002); B. Ashmanskas *et al.*, *ibid.* **518**, 532 (2004).

[22] J. Asaadi, R. Moore, and D. Toback, *Tevatron Timing and Z Collision Distributions For Use in Delayed Photon Analyses*, CDFNote 9812 (2009).

[23] Z. Hong and D. Toback, JHEP **1309**, 041 (2013).